Evaluating the Impact of Spherical Aberration on Sub-0.2-micron Contact/Via Hole Patterning

Shuo-Yen Chou[a], Jen-Chung Lou[a], Chih-Ming Lai[b], Fu-Jye Liang[b], and Li-Jui Chen[b]
[a]Institute of Electronics, National Chiao Tung University, Hsinchu, 300, Taiwan, R. O. C.
[b]Deep Sub-micron Technology Division, ERSO, ITRI, Chutung, Hsinchu, 310, Taiwan, R. O. C.

ABSTRACT

Several super resolution techniques, such as phase-shifting mask (PSM) and off-axis illumination (OAI), have been reported to extend the resolution limit and increase the depth-of-focus (DOF) of optical lithography. However, these techniques provide less immunity to spherical aberration than the conventional approaches like chrome binary mask and low coherent illumination. Best focus position shift is the most well known anomalous phenomenon resulted from spherical aberration. In this paper, the origin of best focus shift is explained in pictorial and analytical forms. The phenomenon is evaluated by observing the exposure-defocus windows of sub-0.2μm hole patterns from an 18% transmission rim-type attenuated PSM combined with several types of illumination. Under high coherent illumination, severe focus shift was observed in sparse patterns as strong phase-shifting effect is applied. For dense hole patterns, OAI results in abrupt focus position variation at specific pattern pitch. The experimental results show that spherical aberration would induce best focus shift, distortion of process windows, loss of DOF, and shrinkage of iso/dense process window overlap. Two approaches were proposed to suppress the impact of spherical aberration. One is introducing proper amount of phase bias in attenuated PSM to adjust the wave aberration in the lens. The other more feasible method is using a customized illumination. A synthesized illumination aperture was proposed to compensate the focus shift. Excellent lithographic performance was obtained in the experiment from this method.

Keywords: contact hole, depth of focus, attenuated PSM, OAI, spherical aberration, best focus shift, quadrupole illumination.

1. INTRODUCTION

As the device dimension scaling down, shorter exposure wavelength and higher NA optics are adopted in exposure system to provide sufficient resolution capability. Due to the high cost of 193nm exposure tools, the 248nm stepper/scanner system with high NA lenses is applied to print sub-0.2μm contact/via hole for 0.15/0.13μm node technologies. According to Rayleigh's equation of depth of focus (DOF), DOF is drastically declined as the lens diameter increases. Several super resolution techniques, such as phase-shifting mask (PSM) and off-axis illumination (OAI), are introduced to retain sufficient DOF while increasing the lens NA at fixed wavelength. For hole pattern formation, attenuated PSM is the most well-known method for enhancing both the image contrast and DOF[1]. A higher transmission attenuated PSM is popular for sub-0.2μm contact delineation because it can provide brighter and sharper image spots to print hole patterns[2-4]. To avoid the undesired side-lobe printing from the high transmission background, rim-type contact design with a Cr shielding layer is recommended in the PSM fabrication. Since the effect of attenuated PSM comes from the interference between mask opening and background to manipulate the amplitude distribution at the pupil, the presence of lens aberration would lead to negative effects on lithographic performance enhancement. As the attenuated PSM for hole patterning has more to do with the DOF than with improved resolution, we focus on the influence of spherical aberration which is the major type of lens aberration to affect the defocus behavior of imaging.

In this paper, we first explain the influence of spherical aberration on the defocus behavior of hole imaging by simple coherent analysis. Experiments with different illumination and mask conditions were taken to validate our explanation. The detrimental effects of spherical aberration on lithographic performance were discussed by examining the exposure-defocus characteristics of sub-0.2μm hole. Feasible methods of alleviating the impact of spherical aberration were also discussed. We elucidated how the influence of spherical aberration depends on illumination schemes by checking the corresponding pupil utilization. After that, a customized illumination configuration can be synthesized to eliminate the impact of spherical aberration without much sacrifice of DOF.

2. EXPERIMENTAL CONDITIONS

A KrF excimer laser stepper with 0.55NA and maximum σ=0.8 was used in this evaluation. A rim-type attenuated PSM whose transmission is 18.9% and averaged phase angle is 181.3° was applied in our experiments. Features for evaluation include a variety of hole arrays whose matrix is 7x7 with different pitches and rim widths. In the lithographic condition setting, different rim widths were assigned to implement various extent of phase-shifting effect. Except for conventional illumination, annular and quadrupole illuminations were also applied to enhance the lithographic performance of dense patterns. The annular configuration has an inner radius of 0.4 and outer radius of 0.8 (annular 1/2). The quadrupole scheme has square illumination poles located at the radius of 0.57 with area of 0.33x0.33. The experimental wafers had 8000Å-thick undoped silicon glass (USG) on silicon. An organic anti-reflective layer was employed to control the reflectivity in resist within 1%. A high-contrast positive-tone chemical amplified photoresist was spin-coated to achieve 0.50μm thickness. The critical dimension (CD) measurements were done using a Hitachi S8820 in-line CD SEM. The measured exposure-defocus data were imported into the ED-Forest™ to extract the experimental DOF at the definition of 7% exposure latitude.

3. IMPACT OF SPHERICAL ABERRATION

1. Best focus shift

The explanation of the influence of spherical aberration on lithographic performance starts with the basic model for a diffraction-limited 1:1 projection system with coherent illumination parallel to the optical axis. Applying Fourier optics and stationary phase approximation[5], the amplitude distribution of image U_i in the vicinity of ideal image plane could be expressed as:

$$U_i = F\left\{ e^{i\frac{2\pi}{\lambda}d\sqrt{1-(\sigma_x^2+\sigma_y^2)}} F\{U_m(x,y)\} \prod\left(\frac{\sqrt{\sigma_x^2+\sigma_y^2}}{NA} \right) e^{i\frac{2\pi}{\lambda}W(\sigma_x,\sigma_y)} \right\} \quad (1)$$

Here, σ_x and σ_y are the direction cosine of the plane waves, and d specifies the defocus position from the ideal image point. U_m represents the mask function. F denotes the Fourier transform operator. W is the aberration function of the projection system. Generally, a complete set of Zernike polynomials is utilized to describe primary and higher order aberration. The polynomials are described by a polar coordinate (ρ, θ), where ρ denotes the pupil radius normalized by the projection lens NA. For the sake of simplicity, we assume the lens aberration is purely spherical. Since the wavefront deviation of spherical aberration is axially symmetrical and independent of the rotation angle θ, the exponential term related to lens aberration in equation (1) could combine with the exponential term of defocus. This indicates spherical aberration will change the defocus behavior of image formation.

In contact mask layout, regular arrays of holes are general and often used as test patterns to evaluate the lithographic performance. Assume the mask layout is an array of square holes with equal pitch p in both x- and y-axis directions, the object spectrum from the Fourier transform of mask function becomes a dot array with pitch λ/p. The discreteness of object spectrum simplifies the Fourier transform of equation (1) to a double trigonometric series. Consequently, the intensity distribution of image, which is the square of the complex amplitude, could be expressed as

$$I(x,y,d) = \sum_{m,n=0}^{\sqrt{m^2+n^2}\le\frac{p\cdot NA}{\lambda}} \sum_{u,v=0}^{\sqrt{u^2+v^2}\le\frac{p\cdot NA}{\lambda}} \alpha_{mnuv} f_{mn} f_{uv} \cos\left(\frac{2m\pi}{p}x\right)\cos\left(\frac{2n\pi}{p}y\right)\cos\left(\frac{2u\pi}{p}x\right)\cos\left(\frac{2v\pi}{p}y\right)$$
$$\times\cos\left(\frac{2\pi}{\lambda}\left(\left(\sqrt{1-\left(m^2+n^2\right)\left(\frac{\lambda}{p}\right)^2}-\sqrt{1-\left(u^2+v^2\right)\left(\frac{\lambda}{p}\right)^2}\right)d+\left(W_{mn}-W_{uv}\right)\right)\right) \quad (2)$$

where $\alpha_{mnuv} = 2^{4-\delta(m)-\delta(n)-\delta(u)-\delta(v)}$ with $m,n,u,v \ge 0$, and $W_{mn} = W(\rho_{mn}) = W\left(\frac{\sqrt{(m^2+n^2)(\lambda/p)^2}}{NA}\right)$

Since the major effect of spherical aberration is on the defocus behavior, we focus on the axis intensity distribution and let x and y coordinates in equation (2) equal zero. Consider the 9-beam interference, that is the imaging by one 0th order, four (±1,0) or (0,±1) orders, and four (±1,±1) orders, the intensity distribution along axis is represented as:

$$I(0,0,d) = f_{00}^2 + 16f_{10}^2 + 16f_{11}^2 + 8f_{00}f_{10}\cos\left(\frac{2\pi}{\lambda}\left(\left(1-\sqrt{1-\left(\frac{\lambda}{p}\right)^2}\right)d+\left(W_{00}-W_{10}\right)\right)\right)$$
$$+8f_{00}f_{11}\cos\left(\frac{2\pi}{\lambda}\left(\left(1-\sqrt{1-2\left(\frac{\lambda}{p}\right)^2}\right)d+\left(W_{00}-W_{11}\right)\right)\right)+32f_{10}f_{11}\cos\left(\frac{2\pi}{\lambda}\left(\left(\sqrt{1-\left(\frac{\lambda}{p}\right)^2}-\sqrt{1-2\left(\frac{\lambda}{p}\right)^2}\right)d+\left(W_{10}-W_{11}\right)\right)\right) \quad (3)$$

where f_{mn} specifies the amplitude of (m,n) diffraction order.

Equation (3) was graphed in figure 1. Each cosine terms that corresponds to the interference of a pair of diffraction orders (plus the DC intensity: $f_{00}^2+16f_{10}^2+16f_{11}^2$) was also plotted in this figure to give a clear visualization of how the defocus behavior varies under the influence of spherical aberration. Since the spherical aberration in a great many optical systems is almost entirely 3rd-order, a 0.02λ 3rd-order spherical aberration is assigned in this illustration. The difference of experienced wave aberration between each pairs of diffraction orders generates a phase constant in the corresponding cosine term. Figure 1(a) shows the case of a binary intensity mask with main feature opening of 0.6λ/NA and pattern pitch of $\sqrt{2}\lambda/NA$. The $f_{00}f_{10}$ and $f_{10}f_{11}$ terms shift to opposite axis directions. As a result, the focus shift in the superposed intensity is smeared due to the offset of these two cosine terms. Compared with the aberration-free axis intensity profile, the asymmetry of axis intensity profile is inconspicuous and the best focus shift is negligible.

On the other hand, there was considerable discrepancy between the defocus behaviors of an attenuated PSM with and without the residence of spherical aberration in the lens (figure 1(b)). Since the attenuated PSM diffracts the 0th order beam f_{00} 180° out of phase than other diffracted beams, the related cosine terms with coefficients of $f_{00}f_{10}$ and $f_{00}f_{11}$ have reverse distributions. As a result, the asymmetry of axis intensity profile is exacerbated. The diffraction focus, which refers to the point with maximum intensity, is apparently deviated from the ideal image point. Hence, a tiny amount of spherical aberration can induce sever focus shift in the application of attenuated PSM. Of course, the phase-shifted 0th order is also the reason of DOF improvement from attenuated PSM. Since attenuated PSM bears weak immunity to spherical aberration, lenses with ultra-low aberrations should be adopted in exposure system when this super resolution technique becomes a necessary tool for low k_1 contact printing.

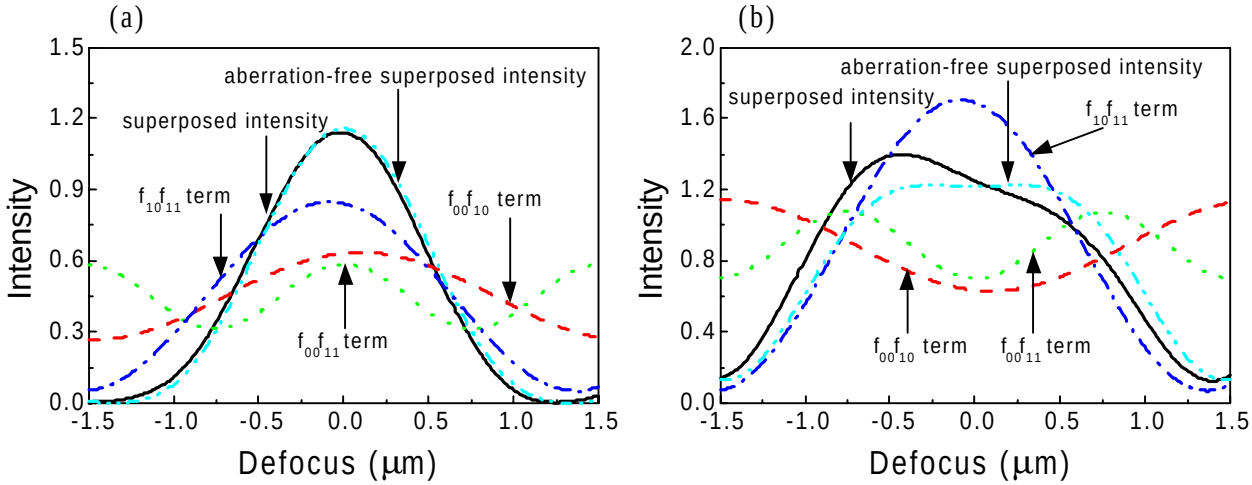

Figure 1: The axis intensity distribution as a function of defocus using (a) a binary intensity mask and (b) an attenuated PSM whose transmittance is 18%. The optical conditions for simulation were 0.55NA and 248nm wavelength.

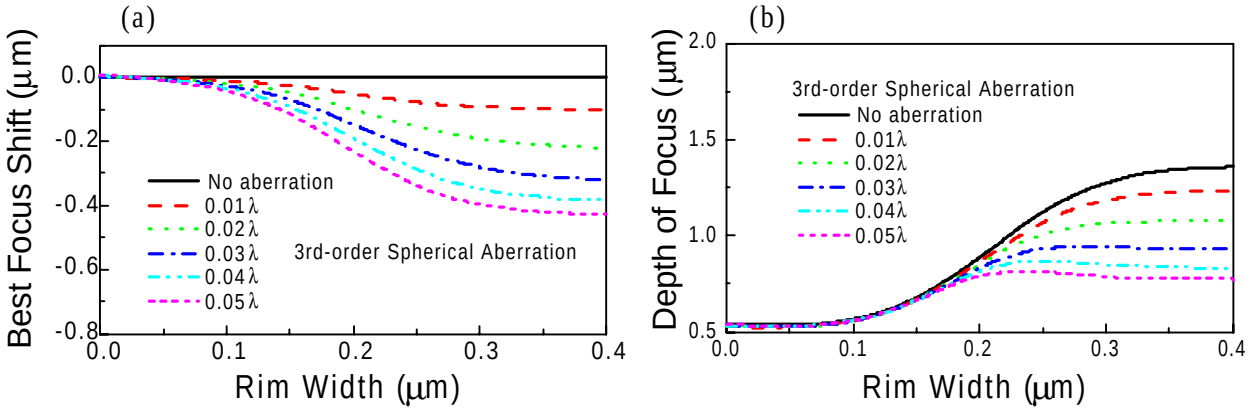

Figure 2: The dependence of (a) best focus position and (b) depth of focus on rim width of 18% transmission attenuated PSM under the influence of spherical aberration. The mask CD is 0.27μm (0.6λ/NA) and the illumination coherence is 0.4.

With the application of higher transmission attenuated PSM, rim-shifter contact design is favored for the purpose of side-lobe intensity suppression. Figure 2 shows the dependence of best focus position and DOF on the rim width of an 18% transmission attenuated PSM under the influence of spherical aberration. The optical condition for simulation is NA=0.55 and illumination coherency=0.4. DOF is defined by the range of 10% intensity loss tolerance, and the best focus position is located at the center of DOF. Without aberration, the focus latitude obtains significant improvement when the rim width is large enough to shift the phase of 0^{th} order beam. A smaller rim width can relieve the focus variation but also dull the DOF enhancement. Figure 3 shows the dependence of best focus position and DOF on CD bias for a halftone PSM (6% transmission). It is indicated that a larger CD bias can suppress the best focus shift at the expense of DOF.

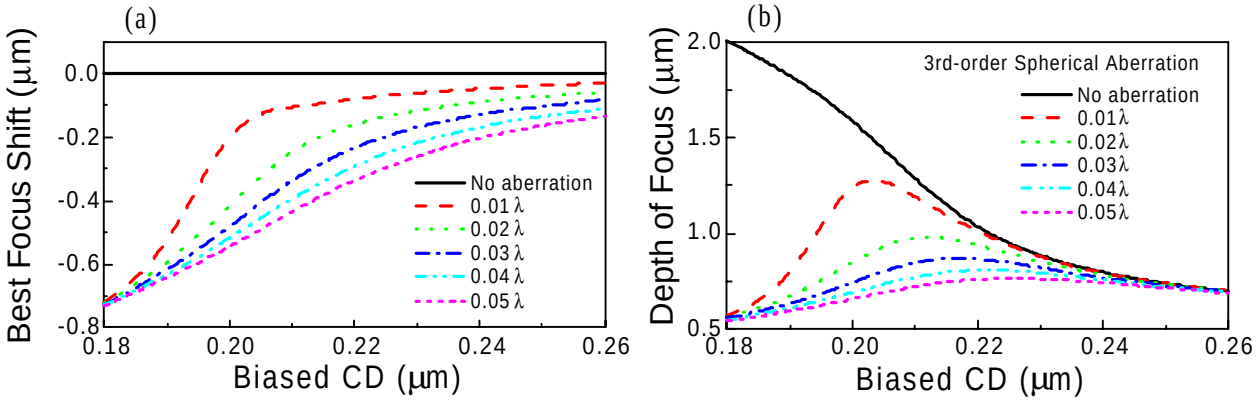

Figure 3: The dependence of (a) best focus position and (b) depth of focus on biased CD under the influence of spherical aberration. The simulation condition is an 6% transmission halftone PSM under conventional σ=0.4 illumination.

2. Process window distortion

In the preceding section, we discuss the impact of spherical aberration on the defocus behavior by observing the axis intensity distribution. However, large exposure latitude is also required to cope with dosage adjustment error and substrate reflectivity variation from device topography or thin film interference. Therefore, it is necessary to evaluate the impact of spherical aberration on the full exposure-defocus windows. Empirically, the exposure latitude is proportion to the image log-slope[6]. Figure 4 compares the image log-slope and central lobe intensity (axis intensity) distribution of a 0.17μm isolated hole as a function of defocus. Without aberration, the best focus position and maximum image log-slope coincide at the ideal image point. As a 0.02λ 3^{rd}-order spherical aberration was added, although the distribution of image log-slope became asymmetrical, its maximum value didn't move along with the central intensity distribution. To explain this anomalous phenomenon, the intensity contour maps of focused field with and without spherical aberration were plotted in figure 5. For contact printing using an attenuated PSM, the emersion of side lobes narrows the central lobe and thus increases the image log-slope. In the ideal case, both central lobe and side lobe have their maximum intensity at the ideal image point (figure 5(a)). However, the existence of spherical aberration split their distribution, as shown in figure 5(b). Hence, the variation of image log-slope doesn't follow the central lobe intensity.

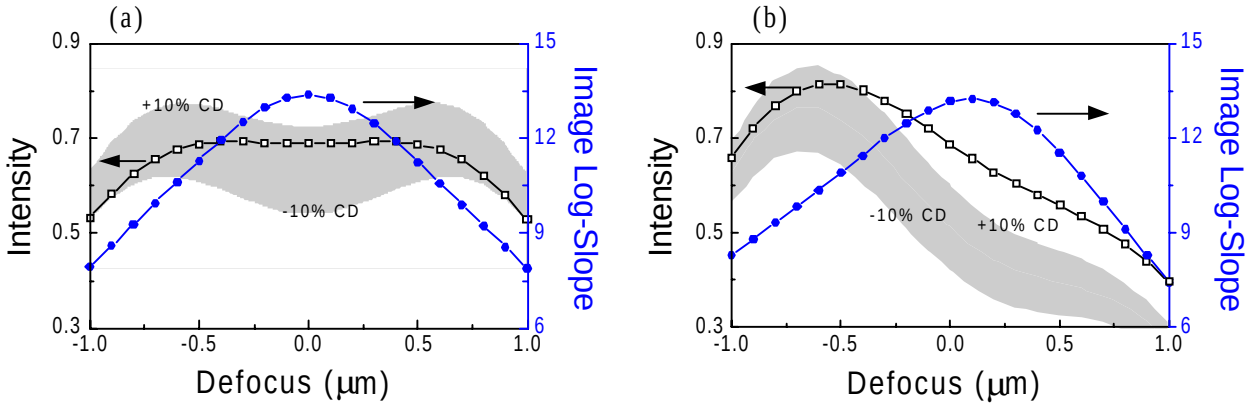

Figure 4: Variation in the central lobe intensity and Image log-slope of 0.17μm hole with respect to the defocus condition. (a) Without aberration. (b) With 0.05λ 3^{rd}-order spherical aberration. The shaded areas indicate the shape of resulting allowed CD space.

The disharmony between the central-lobe intensity and image log-slope reflects on the shape of exposure-defocus window, as illustrated in the shaded area of figure 4. Due to the balance between image intensity and log-slope, the allowed CD space (±10% CD deviation) looks like a skew ribbon so that it's ambiguous to determine the optimum condition for lithographic process. What worse is the skew CD area results in a small overlap with the process windows of other patterns and thus shrinks the common process window.

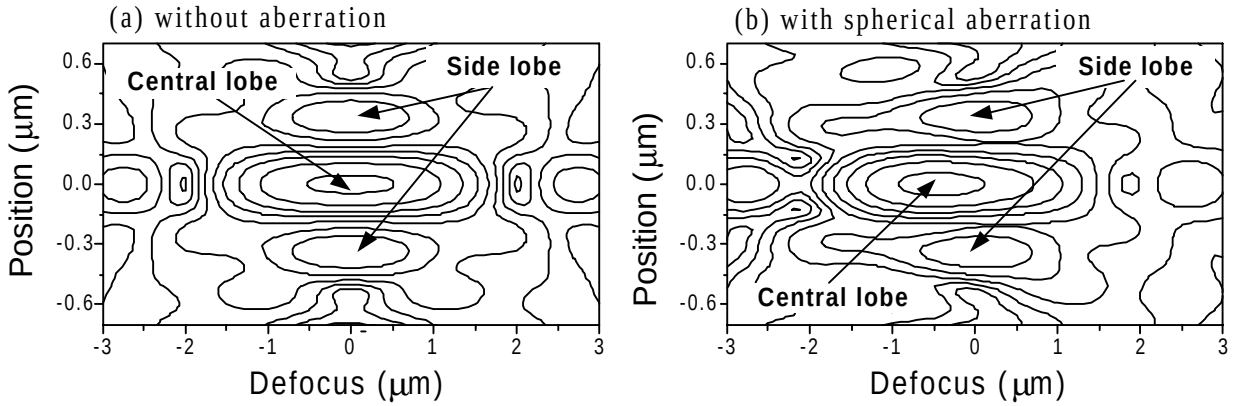

Figure 5: Intensity contour maps of focus field for an isolated contact using attenuated PSM. The optical condition for simulation is NA=0.55 and σ=0.3.

3. Experimental results and discussions

Fig. 6 shows the experimental CD-defocus matrixes of sub-0.2μm isolated contact (pitch=1.70μm). With illumination coherence (σ) of 0.3, a 0.20μm rim-width provided a large DOF with its best focus position at about –0.3μm defocus (figure 6(a)). As the rim-width increased to 0.25μm, the CD-defocus curves became so asymmetrical that its best focus position shifted to –0.7μm defocus (figure 6(b)). As we increased the illumination incoherence to 0.4, the CD-defocus curves of 0.25μm rim width became more symmetrical. Therefore, the best focus shift was reduced and a larger DOF was retained. However, for 0.20μm rim width, the 0.4σ illumination significantly degraded the DOF of 0.17μm hole from 1.5μm to 0.9μm (figure 6(c)). Hence, one should carefully optimize the illumination condition and mask parameters to minimize the influence of aberration. The experimental data shown in figure 6 are summarized in figure 7. It is found a lower illumination coherence can alleviate the best focus shift problem at the sacrifice of DOF. The loss of DOF can be compensated by a larger rim-width. Figure 8 shows the variation of experimental DOF and best focus position with respect to different mask bias. The experimental results indicate the effect of a larger CD bias on best focus shift and DOF is similar to those under a lower degree of illumination coherence.

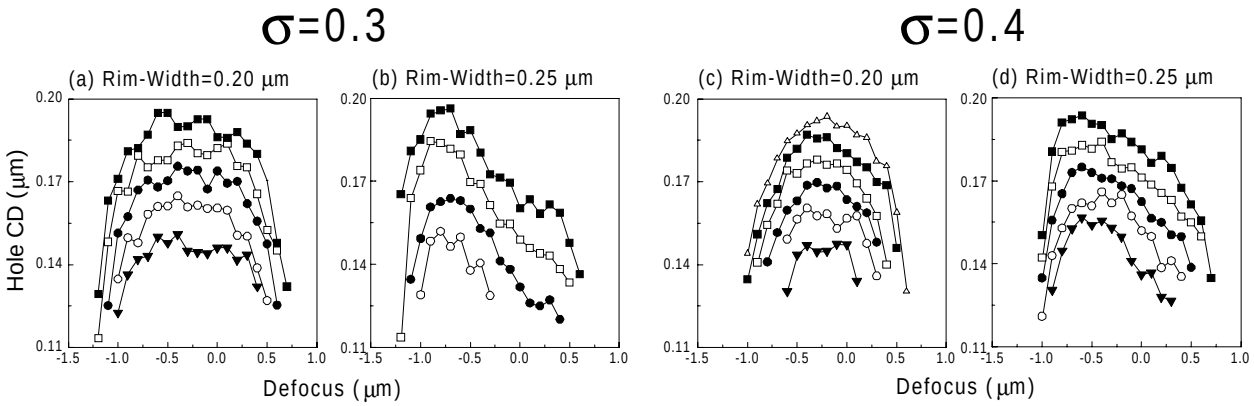

Figure 6: The experimental CD-defocus matrixes of sub-0.2μm isolated hole using 18% transmission rim-type attenuated PSM and 0.55NA optics. The mask CD is 0.27μm (0.6λ/NA).

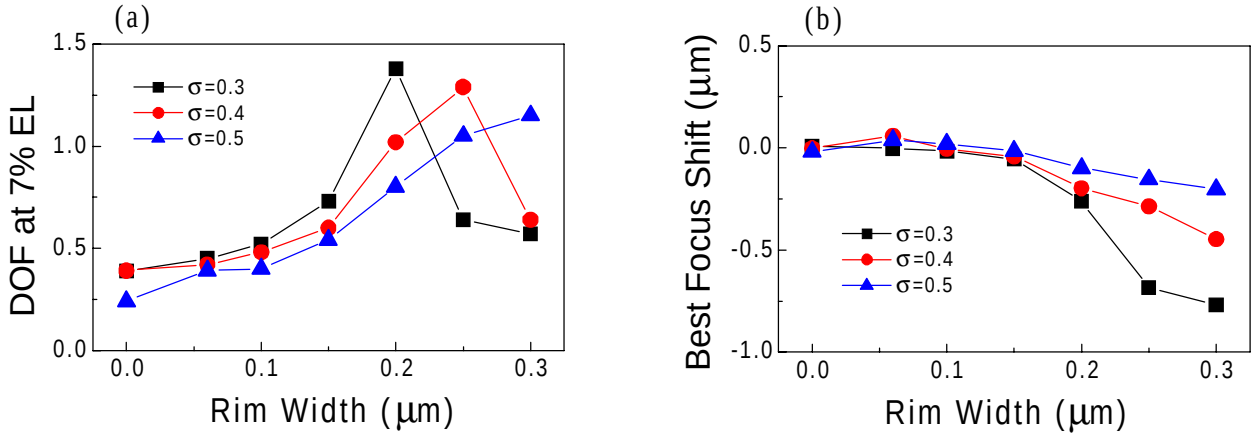

Figure 7: Dependence of (a) experimental DOF and (b) best focus position on rim width with different illumination coherence for 0.17μm hole printing. The mask CD is 0.27μm (0.6λ/NA).

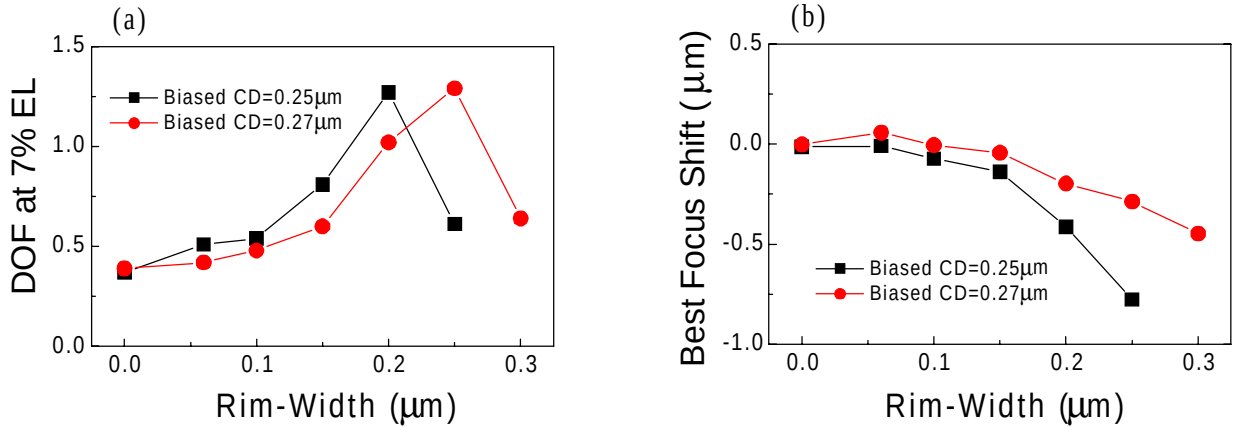

Figure 8: Dependence of (a) experimental DOF and (b) best focus position on rim width with different biased CD in 18% transmission rim-type attenuated PSM. The optical condition is NA=0.55 and σ=0.4.

4. MINIMIZE THE INFLUENCE OF SPHERICAL ABERRATION

1. Phase bias approach

In addition to spherical aberration, phase error, which represents the deviation of optical shift from 180° in phase-shifting structures due to imperfect mask fabrication, also causes the decrease of DOF and best focus shift[7]. Figure 9 shows the distribution of best focus position and DOF in a rim-type attenuated PSM with different phase error. The phenomena shown in figure 9 have similar trends to those shown in figure 2 under the influence of spherical aberration, except the best focus position shift to opposite direction due to the negative phase error. As a result, it is suggested that a proper amount of phase bias (ΔΦ) in shifter material of PSM can offset the effect of spherical aberration on lithographic performance. Figure 10 shows the simulated process windows of 0.17μm isolated contact hole using the resist model. In the ideal condition, a maximum rectangular process window with 1.16μm DOF and 12.3% EL can be drawn in the exposure-defocus space where the CD is within ±10% deviation of the target (figure 10(a)). The residence of a –0.05λ 3rd-order spherical aberration in the projection lens distorts the allowed CD area , so a small process window is due (figure 10(b)). As the mask possesses a -3° phase bias, the allowed CD space becomes much more skew and the process window is further shrunk (figure 10(c)). On the other hand, a positive phase bias can flatten the CD distribution in the exposure-defocus space. Figure 10(f) shows a +10° phase bias can restore the exposure-defocus behavior as if there were no spherical aberration.

Although the phase bias method can reduce best focus shift without the sacrifice of DOF, some practical considerations limit its application in real lithographic process. First, because the condition of lens utilization varies with pattern geometry and illumination schemes, it's difficult to extract a universal phase bias to cover every pattern on the mask. In addition, it's

unpractical and impossible to ask a constant phase bias over the entire mask in the real PSM manufacturing process. Therefore, in the lack of thorough descriptions of lens aberration and accurate phase control technique in PSM fabrication, the phase error should be as small as possible to prevent exacerbating the lithographic performance.

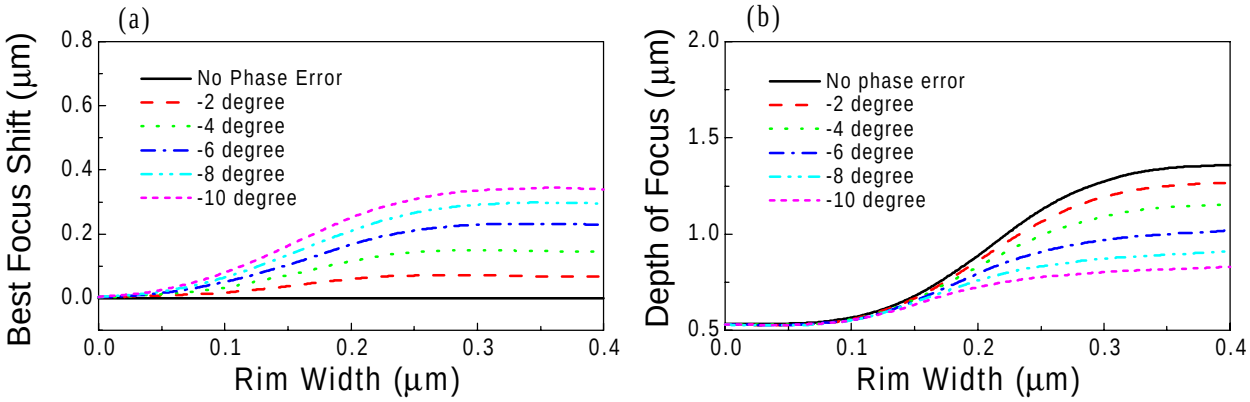

Figure 9: The dependence of (a) best focus position and (b) depth of focus on rim width of 18% transmission attenuated PSM under the influence of phase error. The mask CD is 0.27μm (0.6λ/NA) and the illumination coherence is 0.4.

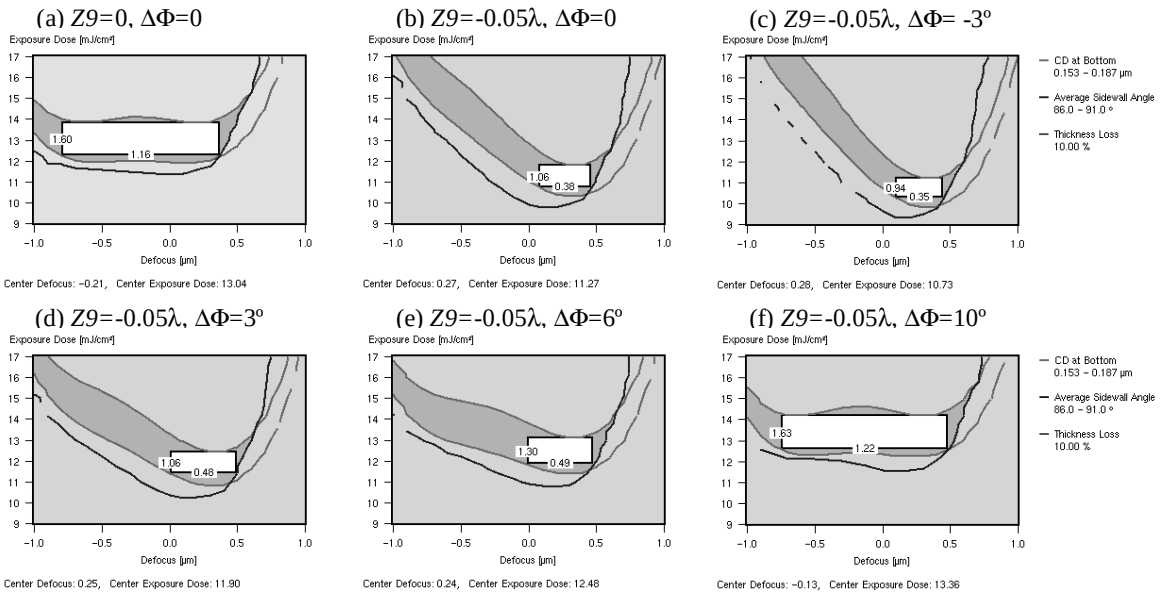

Figure 10: Simulated process windows of a 0.17μm isolated contact under the influence of spherical aberration and phase error.

2. Customized illumination approach

To date, the discussion was concentrated on the lithographic performance of attenuated PSM associated with highly coherent illumination. However, this combination faces serious side-lobe printing problem in dense hole patterning because the optical proximity effect strongly enhances the secondary peak intensity[8]. To push the minimum resolvable pitch as small as possible, off-axis illuminations (OAI) are introduced to catch more $\pm 1^{st}$ order light for imaging. The major benefit of OAI is to improve the DOF of dense pattern by redistribute the diffraction orders at the pupil with equal radial distances from optical axis. Figure 11 shows the experimental DOF and best focus position as a function of pattern pitch using two typical OAI configurations, annular and quadrupole illuminations. The annular illumination, which is a compromised design to fit all pattern orientations, provides no obvious focus position variation through pitches. However, this illumination scheme also results in small DOF through pitches.

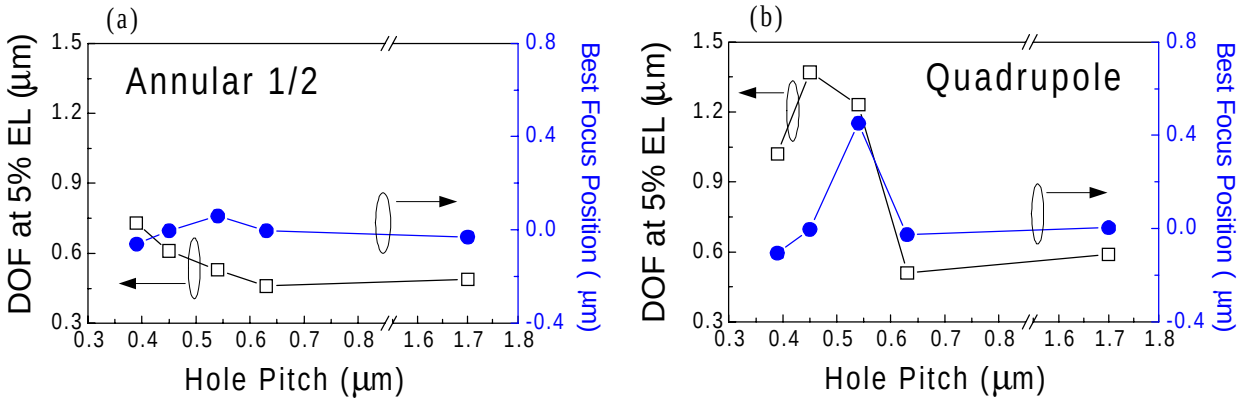

Figure 11: The variation of maximum experimental DOF and best focus position of 0.17μm hole with respect to different hole pitch using (a) annular and (b) quadrupole illumination.

For quadrupole illumination, prominent DOF enhancement is achieved as pattern pitch smaller than 0.64μm. At the same time, the best focus position of 0.54μm pitch moves to +0.45μm defocus. To explain this abrupt focus shift phenomenon, we plotted the illumination chart and source images at the pupil related to 0.54μm and 0.45μm pitches in figure 12 for comparison. The illumination chart was constructed by projecting the pupil image backward into the illumination plane to specify the interference condition from every beam spots of the source. In figure 12(a), the illumination chart shows the quadrupole configuration was all within the four-beam area bounded by (0,0), (±1,0), (0,±1), and (±1,±1) orders. Since the geometry center of the four-beam area indicates the optimum illumination position to distribute the related four diffraction orders symmetrical about the optical axis, the source images of these received diffracted beams largely overlap at the pupil so that a small portion of pupil is utilized for imaging, as shown in figure 12(b). In this condition, a higher order polynomial rather than a simple Zernike function is required to accurately describe the wave aberration in the specific region of the lens[9]. The localization of spatial frequencies emphasizes the variation of wave-aberration at small region of the lens and leads to abrupt focus shift. For 0.45μm pitch, the four illumination poles didn't completely coincide with the four-beam area so that a larger portion of lens pupil was utilized for imaging (figure 12(c) and 12(d)). The experimental results show no best focus shift at this pitch.

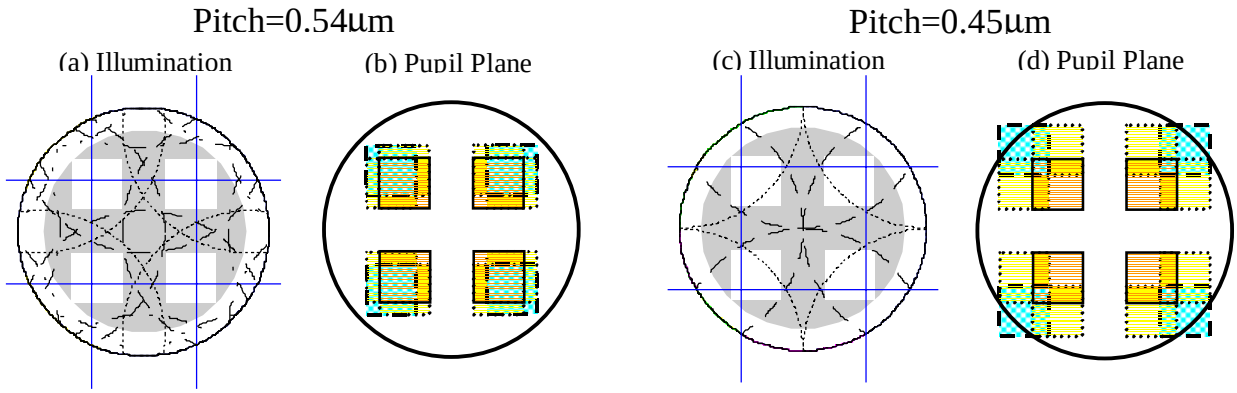

Figure 12: The illumination chart and the pupil utilization for hole pitch of 0.54μm and 0.45μm using quadrupole illumination. The optical conditions are 0.55NA and 248nm wavelength.

The aforementioned discussion suggested the best focus shift in dense hole pattern can be suppressed by a larger portion of lens utilization. Hence, we can customize the illumination configuration to provide better lens utilization without much sacrifice of DOF[10,11]. Figure 13 shows the design of customized illumination, which can be regarded as the combination of conventional highly coherent illumination and quadrupole illumination. According to the experimental data in section 3.3, increasing the partial coherence of illumination can reduce the best focus shift of sparse patterns on attenuated PSM. In our

illumination design, we increase the quadrupole width σ_q to enhance the incoherence of illumination. Figure 14(a) shows the dependence of DOF and best focus position of a 0.17μm isolated contact on quadrupole width. At first, the DOF increases with the quadrupole width because higher illumination incoherence makes the CD-defocus behavior more symmetrical so that a larger process window can be defined. However, too large quadrupole width would dull the DOF performance because the attenuated PSM favors high coherent illumination. The best focus shift is prominent reduced as the quadrupole width increases. Figure 14(b) shows the effect of quadruple width on DOF and best focus position for dense hole patterns with pitch of 0.54μm. Although the customized illumination can't provide extremely large DOF at this pitch as quadrupole illumination does, it effectively suppresses the best focus shift. With the view of a large common iso/dense process window, our customized illumination provides better lithographic performance than those from quadrupole or conventional illumination. The experimental results in figure 14 show a quadrupole width of 0.3 is an optimum design to minimize best focus shift and preserve sufficient DOF.

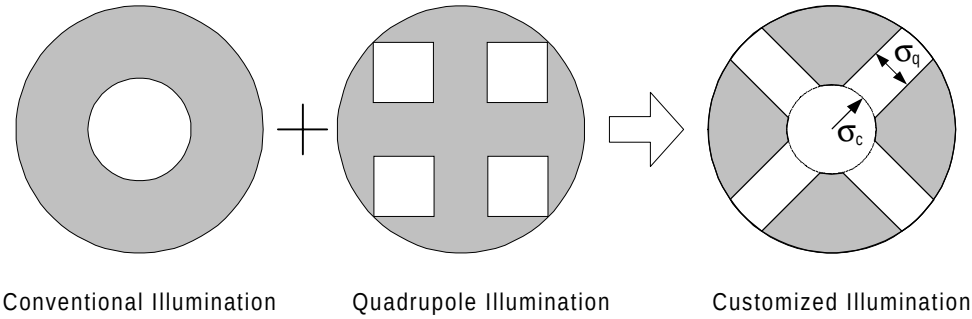

Figure 13: Concept of customized illumination design. The synthesized illumination configuration can be described by two parameters: σ_c and σ_q.

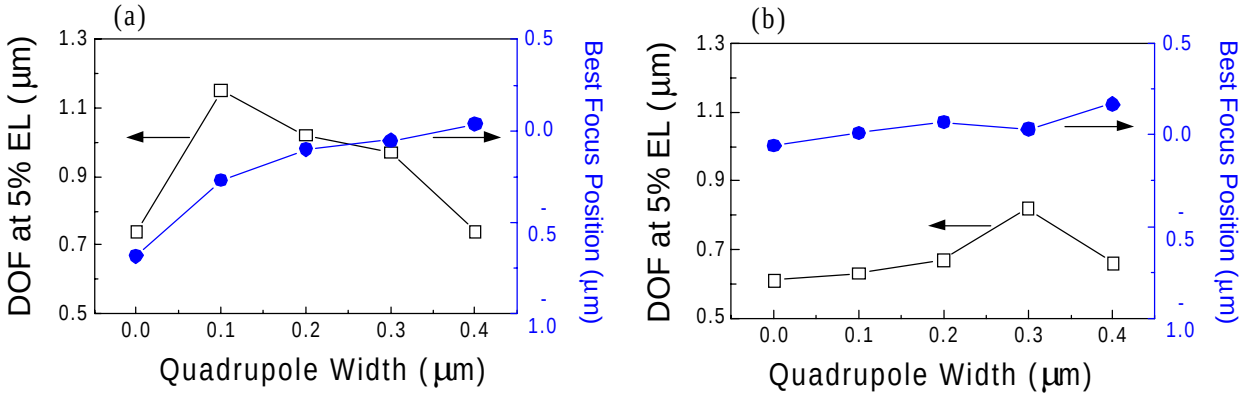

Figure 14: The variations of DOF and best focus position of 0.17μm with respect to different quadrupole width of customized illumination. The center illumination pole (σ_c) has a radius of 0.3. (a) Iso contact of 1.70μm pitch with mask CD=0.27μm and rim-width=0.25μm. (b) Dense contact of 0.54μm pitch with mask CD=0.25μm and attenuated background.

5. CONCLUSIONS

In this paper, we thoroughly study the influence of spherical aberration on sub-0.2μm contact printing. The attenuated PSM inherits weak immunity from spherical aberration than conventional Cr mask. It is found the spherical aberration can induce best focus shift, loss of DOF, and common process window shrinkage. Experimental results suggest a larger CD bias, a smaller rim-width, and higher degree of partially coherent illumination can suppress the best focus shift at the expense of DOF. Phase bias method can eliminate the best focus shift without loss of DOF. However, the optimum phase angle is difficult to extract, and accurate phase control is required in mask manufacturing. A useful illumination scheme is proposed to suppress the impact of spherical aberration. Although the individual DOF is degraded under the customized illumination,

the reduction of best focus shift increases the overlap of iso/dense process windows. The customized illumination method is the most feasible approach to reduce the impact of spherical aberration.

ACKNOWLEDGMENTS

The author would like to thank all colleagues ever in S200 ERSO for their consistent encouragement and useful discussions.
.

REFERENCE

1. T. Terasawa, N. Hasegawa, H. Fukuda, and S. Katagiri, “Imaging Characteristics of Multi-Phase-Shifting and Halftone Phase-Shifting Masks”, Jpn. J. Appl. Phys. **30**, 2991 (1991)
2. H. Iwasaki, K. Hoshi, and H. Tanabe, “High Transmittance Rim-type Attenuated Phase Shift Masks for Sub-0.2μm Hole Patterns”, Proc. SPIE **3412**, 601 (1998)
3. R. J. Socha, J. S. Petersen, F. Chen, T. Laidig, K. Wampler, and R. Caldwell, “Design of 200nm, 170nm, 140nm DUV Sweeper High Transmission Attenuating Phase Shift Mask through Simulation Part I”, Proc. SPIE **3546**, 617 (1998)
4. N. Kachwala, J. S. Petersen, and M. McCallum, “High Transmission Attenuated PSM – Benefits and Limitations through a Validation Study of 33%, 20%, and 6% Transmission Masks”, Proc. SPIE **4000**, 1163, (2000)
5. M. Mansuripur, “The Physical Principles of Magneto-optical Recording”, Chap. 3, Cambridge University Press, 1995
6. C. Mack, “Inside Prolith”, Chap. 10, FINLE technologies, 1998
7. J. Miyazaki, A. Nakae, H. Kusunose, N. Yoshioka, W. Wakamiya, and K. Murayama, "Effect of Phase Error on Lithographic Characteristics Using Attenuated Phase-Shifting Mask", Jpn. J. Appl. Phys. **33**, 6785 (1994)
8. H. Shimizu, F. Uesawa, T. Oda, and M. Sugawara, “Experimental Verification of an Aerial Image Evaluation Method and Its Application to Studies of Attenuated Phase-Shifting Masks”, Jpn. J. Appl. Phys. **34**, 6598 (1995)
9. S. Nakao, A. Nakae, J. Sakai, T. Miura, S. Tatsu, “Measurement of Spherical Aberration Utilizing an Alternating Phase Shift Mask”, Jpn. J. Appl. Phys. **37**, 5949 (1999)
10. C. C. Hsia, T. S. Gau, C. H. Yang, R. G. Liu, C. H. Chang, L. J. Chen, C. M. Wang, J. F. Chen, B. W. Smith, G. W. Hwang, J. W. Lai, and D. Y. Goang, “Customized Off-axis Illumination Aperture Filtering for sub-0.18μm KrF Lithography”, Proc. SPIE **3679**, 427, (1999)
11. T. S. Gau, R. G. Liu, C. K. Chen, C. M. Lai, F. J. Liang, and C. C. Hsia, “The Customized Illumination Aperture Filter for Low k1 Photolithography Process”, Proc. SPIE **4000**, 271, (2000)